Supporting Information

Control of Near-infrared Dye Fluorescence Lifetime in All-Polymer Microcavities

Heba Megahd,[a] Mariela Villarreal Brito,[a] Andrea Lanfranchi,[a] Paola Stagnaro,[b] Paola Lova,[a] Davide Comoretto[a*]

a. Dipartimento di Chimica e Chimica Industriale, Università di Genova, Via Dodecaneso 31, 16146 Genova, Italy

b. Istituto di Scienze e Tecnologie Chimiche "Giulio Natta", Consiglio Nazionale delle Ricerche, SCITEC-CNR, Via de Marini,6, 16149 Genoa, Italy

*davide.comoretto@unige.it

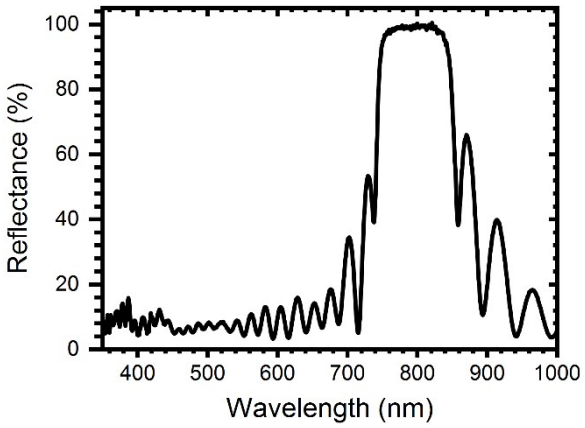

Figure S1: Reflectance of the bottom DBR for MC_{tuned}

The reflectance of the bottom DBR in Fig. S1 shows a great similarity to that of the tuned microcavity shown both in the main text and in Fig. S2 below. The first order extends from approximately 744 nm to 855 nm, with a FWHM of around 111 nm, comparable to that of the MC_{tuned} in the main text (120 nm). As the structure is a highly uniform dielectric mirror, the absence of cavity modes and splitting of the interference fringes is self-evident.

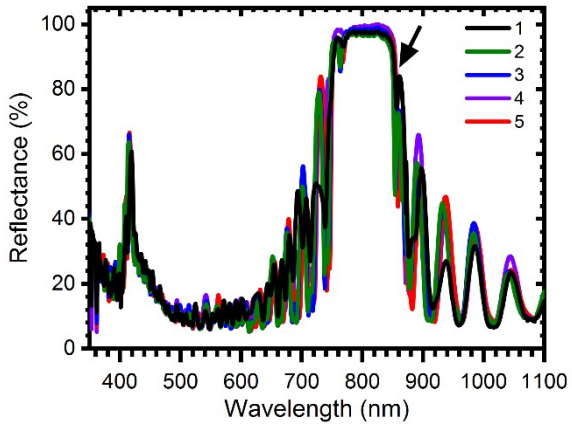

Figure S2: Reflectance of different spots of MC_{tuned}

The reflectance spectra of MC_{tuned} at different spots in Fig. S2 clearly shows the main microcavity mode at an average value of 858 nm (black arrow). The spectral positions and intensities of the fringes, the PBG and the wavelength of the cavity modes is highly uniform between the different spots with a maximum shift below 10 nm.

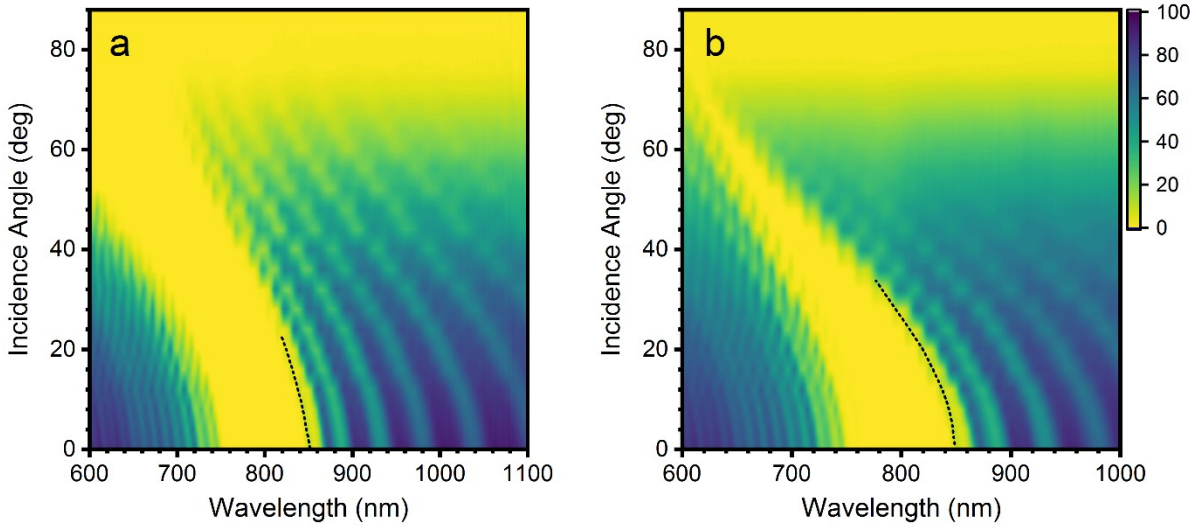

Figure S3: Angle-resolved transmittance of (a) S and (b) P polarization for MC_{tuned}. The dashed line highlights the dispersion of the cavity mode.

Due to the photonic band structure of the microcavity, the transmittance spectrum depends strongly on the incidence angles, as well as the polarization of the incident light. Panels a and b of Fig. S3 show the experimental angle-resolved transmittance spectra collected for S and P polarizations, respectively. The yellow values represent low transmittance, and the cooler blue hues represent high transmittance. As such, the yellow wide bands that are shifting to lower wavelengths as the collection angle increases represent the PBG, while the light green line (see black dotted line) that starts around 850 nm at normal collection is the dispersion main microcavity mode. For the S-polarization no significant effects on the PBG width are observed, while for the P-polarized transmittance the PBG narrows at the Brewster's angle.

For a rough estimation of the complex effective refractive index of the Dye:PAA blend, we use the absorption of a film of the NIR dye blended in PAA (with the same concentration and thickness as for the microcavity) in the (600-900 nm) wavelength window to calculate the extinction coefficient (k) of the blend.

The value of absorption of the thin film is first corrected for the reflectance at the interface between the film and air. Then, k can be estimated from the absorption of the Dye:PAA film ($k = \frac{\alpha\lambda}{4\pi}$), where α is the absorption coefficient.

The dispersion of α and n can be approximately described by the simplified Kramers–Kronig dispersion relations in equation (1) and (2) for frequencies ω in the neighborhood of a molecular transition frequency ω_0.[1] In the equations, N is the number of dipoles per unit volume, m_e is the mass of the electron, e is the elementary charge, ε_0 is the permittivity of free space, c is the speed of light and Γ is the damping factor. As multiple transitions can occur in molecular dyes, a summation of Lorentzian functions is needed to reflect this.

$$\alpha = \frac{N e^2}{m_e c \varepsilon_0} \sum_j \frac{\Gamma_j}{4(\omega_{j0} - \omega)^2 + \Gamma_j^2} \#(1)$$

The fitting parameters are reported in Table S1.

Table S1. Fitting parameters for absorption

Transition	ω_0(10^{15} s^{-1})	Γ(10^{14} s^{-1})
Principal transition	2.43	1.27
Secondary	2.65	2.73

The effect of the absorption on the general shape of the real part of the refractive index can be described by anomalous and negative dispersion using the fitting parameters obtained by Lorentzian fitting of the absorbance reported in Table S1 in Equation (2).[1]

$$n = 1 + \frac{N e^2}{m_e \varepsilon_0 \omega_0} \sum_j \frac{(\omega_{j0} - \omega)}{4(\omega_{j0} - \omega)^2 + \Gamma_j^2} \#(2)$$

It is possible to approximate the effective refractive index and extinction coefficient of the Dye:PAA blend using their weighed averages, using the fitted complex refractive index of the blend and that of PAA reported in the literature[2] to roughly estimate the values as shown in Fig.S4.

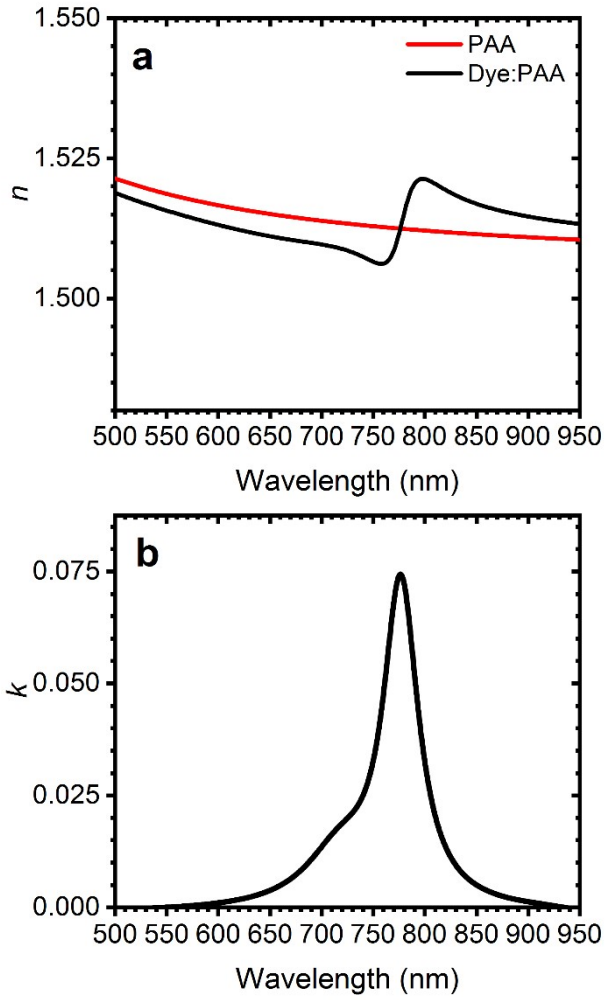

Figure S4. Estimated complex refractive index $n + ik$ (n, panel **a**; k, panel **b**) dispersion for the Dye:PAA blend.

Figure 5a shows the transmittance measured at normal angle and the corresponding photoluminescence at the same spot in panel b. The cavity mode corresponding to the increased transmittance at approximately 850 nm (dashed line) is perfectly spectrally tuned to the measured PL enhancement.

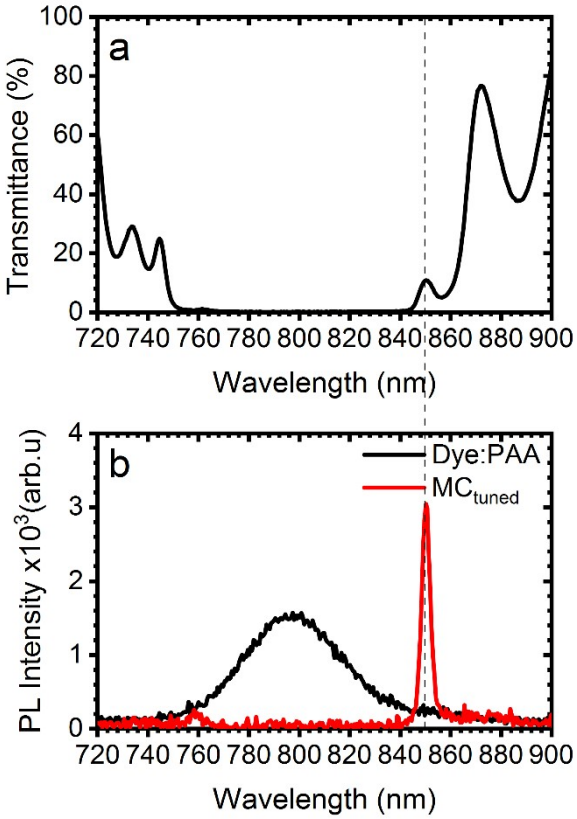

Fig. S5: Perfect correspondence of cavity mode measured in transmittance (a) and enhanced PL peak of the MC_{tuned} (b).

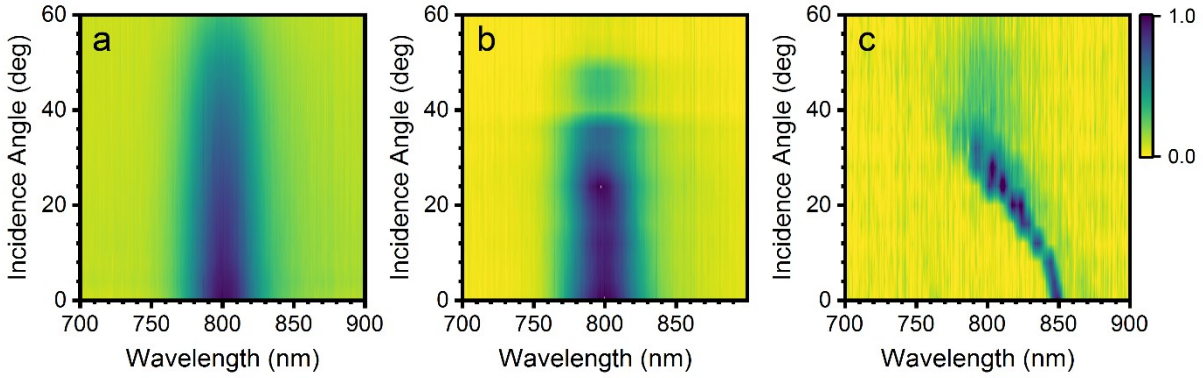

Figure S6. Angle-resolved emission for (a) Dye:PAA, (b) $MC_{detuned}$ and (c) MC_{tuned}

Figure S6 compares contour plots of the emission spectra of the standalone Dye:PAA film and the cavities as a function of the incidence angle, where the blue hues indicate higher emission intensity. The angle resolved emission of the Dye:PAA layer is evidently influenced by its inclusion in the microcavities. The standalone Dye:PAA film shows no angular dependence when it comes to the spectral position of the emission peak, only a decrease in intensity as the angle of incidence is increased, as expected. In the case of $MC_{shifted}$, the emission intensity is modulated by filtering effects from the interference fringes of the DBRs, while no angular dispersion of the spectrum is observed. On the other hand, the emission from MC_{tuned} is completely altered, showing a narrowing of the emission band to the cavity mode (the enhancement effect discussed in the manuscript), which continuously shift in the emission peak wavelength to higher energies as the angle is increased. This fits with the observation of the angle-resolved transmittance, where both the PBG and the cavity mode shift to longer wavelengths.

Table S2 Biexponential fitting parameters for lifetimes of Dye:PAA layer, $MC_{detuned}$ and MC_{tuned}

Parameter	Dye:PAA	MC_{tuned}	$MC_{detuned}$
I_1 (Counts)	512	870	851
τ_1 (ns)	1.1	2.9	1.9
I_2 (Counts)	1640	3935	3585
τ_2 (ns)	0.27	0.39	0.36

Each decay curve was fitted with a biexponential function ($I(t) = I_1 e^{-(\frac{t}{1})} + I_2 e^{-(\frac{t}{\tau_2})}$). The lifetimes were averaged considering their intensity ($\tau_{av} = \frac{\sum_i I_i \tau_i^2}{\sum_i I_i \tau_i}$),[3] which allowed to determine the overall decay process of the emitter embedded in the microcavities and for the emitter blend.

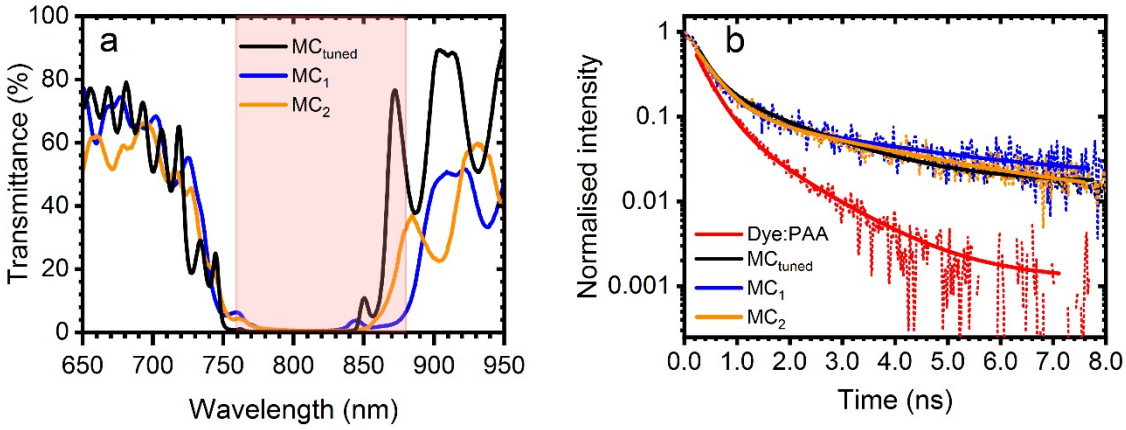

Figure S7: (a) Transmittance spectra of microcavities with different cavity lengths and similar cavity mode wavelengths, (b) PL decays of the microcavities compared to a reference layer of Dye:PAA.

In order to investigate the reproducibility of the observed effect, different cavities with similar PBGs and primary MC mode wavelengths (MC_{tuned}, MC_1 and MC_2) were fabricated and characterized. All the microcavities consist of 2 DBRs of 20 BLs each, sandwiching a layer of the Dye:PAA blend. However, the thickness of the PVK layers in the direct vicinity of the active layer are varied. Table S3 lists all the samples, their cavity length (L_c~PVK_{above}+PVK_{below}+Dye:PAA), principal cavity mode wavelength (λ_c), η, τ_{av} and Γ_{rad}. The transmittance of each sample is reported in Figure S7a, with all samples showing a PG tuned to the Dye emission (red shaded area), with a MC mode around 840-850 nm. The lifetime measurements are shown in panel b. The thickness of the layers was estimated through atomic force microscope measurements using the scratch method on thin films on glass substrates cast under the same conditions as the cavities. Clearly, the quantum yields and average PL lifetimes for the three samples are very similar, and consequently their radiative lifetimes is identical within the margins of error.

Table S3: Characterization of various microcavities

Parameter	L_c (nm)	λ_c(nm)	η (%)	τ_{av} (ns)	Γ_{rad}.(ns^{-1})
MC_{tuned}	620	850	5± 2	1.9	0.5
MC_1	900	844	6 ± 2	1.9	0.5
MC_2	920	860	7 ± 2	2.0	0.5

In order to have a concrete understanding of the effect of refractive index contrast between the polymers used for the dielectric mirrors, we make a comparison of hypothetical structures with the same tuning and comparable thicknesses. The polymer pairs chosen are PS/CA (Δn=0.109), PVK/CA (Δn=0.212), PVK/PAA (Δn=0.197), where the refractive indices of the materials are approximately n_{PS}=1.58, n_{PVK}=1.68, n_{CA}= 1.47, n_{PAA}=1.48, and n_{AQ}=1.35 in the NIR spectral range. The pairs were picked as in literature they constituted microcavities that demonstrated emission intensity enhancement but not radiative rate modification.[2, 4-7] To simulate the structures that contain PVK, its thickness was kept constant while the thickness of the low-index material was varied to position the microcavity mode at 850 nm (CA= 147 nm and PAA= 148.5 nm). For the PS/CA pair, CA was kept at 147 nm, and the thickness of the high-index PS was changed accordingly (123.5 nm) while the defect layer was not changed for all simulations. As such, the overall thickness of the simulated samples is similar, at about 10 μm.

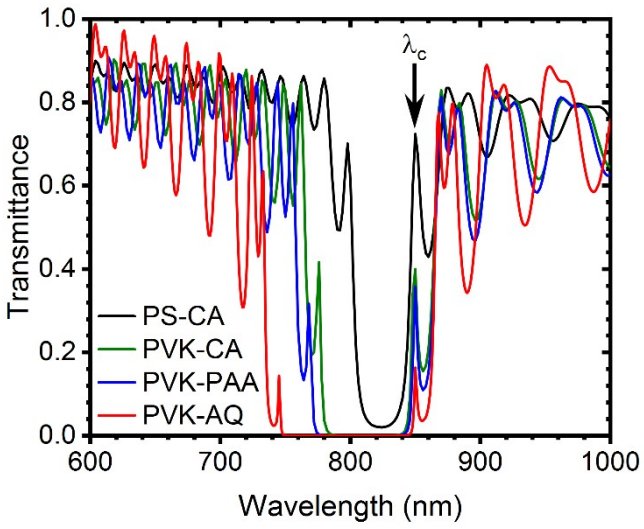

Figure S8. Simulated transmittance for microcavities using different polymer pairs for the DBRs.

The results of the transfer matrix method calculations of the transmittance of all structures using discretization of wavelength of 1 nm are shown in Fig. S8. The low dielectric contrast between the PS and CA results in a planar microcavity with a PBG that fails to reflect 100% of the incident light, with a transmittance of about 2%). For PVK/CA and PVK/PAA based microcavities with a comparable refractive index thickness difference, the transmittance of the PBG is zero with a wider band than that for PS/CA, but less narrow than that of PVK/AQ. Hypothetically, using a pair of higher refractive index such as PVK/Hyflon, would result in even wider PBGs and higher confinement, however the processability of Hyflon is much lower than that here observed for AQ.[8, 9] This simulation was used to compare the relative intensity of the electric field at the microcavity mode wavelength for the different structures as well as the width of the photonic bandgap as reported in the main text.

References

1. W. Demtröder, in *Laser Spectroscopy: Basic Concepts and Instrumentation*, ed. W. Demtröder, Springer Berlin Heidelberg, Berlin, Heidelberg, 1996, DOI: 10.1007/978-3-662-08260-7_3, pp. 57-98.
2. P. Lova, V. Grande, G. Manfredi, M. Patrini, S. Herbst, F. Würthner and D. Comoretto, All-polymer photonic microcavities doped with perylene bisimide j-aggregates, *Adv. Opt. Mater.*, 2017, **5**, 1700523.
3. A. Sillen and Y. Engelborghs, The Correct Use of “Average” Fluorescence Parameters, *Photochem. Photobiol.*, 1998, **67**, 475-486.
4. P. Lova, M. Olivieri, A. Surace, G. Topcu, M. Emirdag-Eanes, M. M. Demir and D. Comoretto, Polymeric Planar Microcavities Doped with a Europium Complex, *Crystals*, 2020, **10**, 287.
5. G. Manfredi, P. Lova, F. Di Stasio, R. Krahne and D. Comoretto, Directional Fluorescence Spectral Narrowing in All-Polymer Microcavities Doped with CdSe/CdS Dot-in-rod Nanocrystals, *ACS Photonics*, 2017, **4**, 1761–1769.
6. L. Frezza, M. Patrini, M. Liscidini and D. Comoretto, Directional enhancement of spontaneous emission in polymer flexible microcavities, *J. Phys. Chem. C*, 2011, **115**, 19939 - 19946.
7. V. M. Menon, M. Luberto, N. V. Valappil and S. Chatterjee, Lasing from InGaP quantum dots in a spin-coated flexible microcavity, *Opt. Express*, 2008, **16**, 19535-19540.
8. P. Giusto, P. Lova, G. Manfredi, S. Gazzo, P. Srinivasan, S. Radice and D. Comoretto, Colorimetric detection of perfluorinated compounds by all-polymer photonic transducers, *ACS Omega*, 2018, **3**, 7517-7522.
9. *WO Pat.,* WO2016087439A1, 2016.